Bulletin of Earthquake Engineering (2021) 19:241–262
https://doi.org/10.1007/s10518-020-00983-0

ORIGINAL ARTICLE

Performance evaluation of buckling-restrained braced frames under repeated earthquakes

Nader Hoveidae[1] · **Saeed Radpour**[1]

Received: 15 August 2020 / Accepted: 10 October 2020 / Published online: 27 October 2020

Abstract
Structures in earthquake-prone areas are not subjected to a single seismic event, but also to a seismic sequence consisting of mainshock and several aftershocks. However, the influence of seismic sequence on performance of structures has not been addressed in majority of existing seismic codes. This paper investigates the effect of repeated earthquakes on performance of steel buckling restrained braced frames. For this purpose, 4-story and 10-story prototype buckling restrained braced frames, designed according to Iranian building codes, are exposed to five seismic sequences. Nonlinear time history analyses are conducted and the responses of frames are measured in terms of maximum inter-story and residual drifts. Furthermore, Park–Ang damage indices and global ductility factors are obtained for braced frames under examined mainshocks and mainshock–aftershock sequences. From the results of this research, it is found that the seismic sequence has the potential to increase the inter-story drift, residual drift, damage index and global ductility factor of buckling restrained braced frames. It is also highlighted that the spectral acceleration of mainshock–aftershock sequence, in comparison to that of single event mainshock, considerably affects the performance of buckling restrained braced frame under repeated earthquakes.

Keywords Seismic sequence · Buckling restrained brace · Inter-story drift · Residual drift · Seismic damage · Global ductility factor

1 Introduction

Buildings located in high-seismic regions are subjected to repeated earthquakes rather than a single seismic event. Generally, contemporary seismic code regulations are based on design earthquake and do not consider the repeated earthquake phenomena. However, past studies have shown that the structural response and damage may be significantly increased due to seismic sequence, since the rehabilitation procedure between seismic sequences cannot be essentially possible due to lack of time. During an earthquake, aftershock events

✉ Nader Hoveidae
Hoveidaei@azaruniv.ac.ir

Saeed Radpour
S.Radpour@azaruniv.ac.ir

[1] Civil Engineering Department, Azarbaijan Shahid Madani University, Tabriz, Iran

are triggered by the mainshock due to both static stress and dynamic stress variations (Aki 1984; Dalguer et al. 2002). Particularly, seismologists have stated that following the mainshock, the aftershocks occurs due to rupture of asperities and barriers in a fault (Ruff and Kanamori 2003). Historical earthquakes have revealed that the aftershocks are able to rise the damage state at the end of the mainshock. The significant residual displacements after the mainshock may result in technical difficulties in repairing of buildings, which can be considered as an upcoming threat due to the aftershock.

Several past studies have paid attention to the influence of seismic sequence on performance of structures. Seismic response of single-degree of freedom (SDOF) systems under repeated earthquakes have been widely investigated (Mahin 1980; Amadio et al. 2003; Luco et al. 2004; Hatzigeorgiou and Beskos 2009; Hatzigeorgiou 2010). Furthermore, the seismic response of multi-degree of freedom systems was studied by several researchers (Fragiacomo et al. 2004; Lee and Foutch 2004; Li and Ellingwood 2007). Hatzigeorgiou and Liolios (2010) studied the seismic response of reinforced concrete frames under five as-recorded and 40 artificial seismic sequences and it was found that the ductility demands were increased due to repeated earthquakes. Garcia and Manriquez (2011) studied the effect of seismic sequence on response of steel moment resisting frames in Mexico and it was resulted that, in contrast to previous studies, as-recorded aftershocks do not considerably increase residual and peak inter-story drift demands. Furthermore, Loulelis et al. (2012) investigated the seismic response of steel moment resisting frames subjected to a set of as-recorded and synthetic seismic sequences and they found that the peak inter-story and residual drifts of steel frames were increased due to the recurrence of earthquakes. Moreover, Garcia (2012) observed that the response of structures under as-recorded real seismic sequences is very different from that of artificial sequences. It was also found that the post-mainshock response of structures is significantly influenced by predominate period of aftershock.

A numerical approach for estimating the effects of repeated earthquakes on seismic response of structures strengthened by cable-elements was proposed by Liolios et al. (2013).

Martinez et al. (2014) assessed the response of two steel moment resisting frames subjected to artificial seismic sequences, where it was observed that the inter-story drifts were significantly increased due to seismic sequence.

The response of tall RC buildings strengthened by cables and subjected to multiple earthquakes was investigated by Liolios et al. (2015). Furthermore, behavior of steel frames equipped with buckling restrained brace (BRB), subjected to seismic sequences, was investigated by Guerrero et al. (2017). It was found that the effect of aftershocks on response of dual buckling restrained braced frames is significant when the peak ground velocity (PGV) of the aftershock is similar to that of mainshock. Moreover, three-dimensional response of steel moment resisting buildings under seismic sequences were studied by Garcia et al. (2018). This study revealed that the modelling method in 3-D models has major influence in seismic response of steel framed-buildings under seismic sequences. It was also demonstrated that 3-D building models experience different response than the 2-D model. It was also shown that the seismic response is different, with differences depending on the angle of incidence of the orthogonal components of the seismic sequences and the number of stories.

The effect of earthquake recurrence on response modification factor of steel moment-resisting frames was investigated by Abdollahzadeh and Sadeghi (2018). Another research by Morfuni et al. (2019) on dual systems equipped with BRBs showed that BRB's capacity could be potentially affected by earthquake recurrence.

Buckling Restrained Braces exhibit a balanced hysteretic response by axial yielding under tension and compression forces during severe earthquakes. Compared with other seismic energy dissipation systems like conventional steel braces or cable (only-tension) bracing system (Massumi and Absalan 2013), BRBs possess several advantages like relatively low-cost construction, easy fabrication, inspection and replacement after severe damages.

BRBs are usually used for the seismic upgrading of existing framed systems, steel or reinforced concrete (RC) ones and so they constitute a dual system with the original frame. Furthermore, a study by Hoveidae and Habibi (2019) indicated that BRBs significantly enhance the progressive collapse capacity of steel moment resisting frames.

Several past studies have demonstrated that BRBs act like a ductile fuse member, producing significant ductility and energy dissipation capacity (Merrit et al. 2003; Black et al. 2000; Tremblay et al. 2006). In a typical BRB, local buckling of the core member and global buckling of the entire brace are inhibited by a restraining mechanism. During past decades, a number of experimental and theoretical studies have focused on seismic response of BRBs. Sabelli et al. (2003) investigated the seismic demands on BRBs through nonlinear time history analysis of braced frames. Hoveidae and Rafezy (2012) investigated the global buckling behavior of all-steel BRBs through finite element analysis method. Guo et al. (2017) proposed a new type of BRBs called core-separated buckling-restrained brace (CSBRB) and theoretically and experimentally investigated the behavior of the brace. Fahnestock et al. (2007) performed nonlinear analyses on a 4-story BRB frame and determined the mean maximum residual story drifts as 0.5 and 1.2% under DBE and MCE ground motion ensembles, respectively.

Component testing of steel-core buckling restrained braces with pinned end connections was conducted by Celik et al. (2015). Avci-Karatas et al. (2018) experimentally examined the seismic response of aluminum-alloy and steel core buckling restrained braces. Moreover, Avci-Karatas et al. (2019) studied the modeling of BRBs using full-scale experimental data.

Majority of prior studies on BRBs concentrate on detailing and seismic response of buckling restrained braced frames (BRBFs) under single earthquake phenomenon. However, BRBFs in seismic-prone zones may be exposed to multiple earthquake events. Unlike steel moment-resisting frames, only a handful of studies have focused on performance of BRBFs under earthquake recurrence (Guerrero et al. 2017; Morfuni et al. 2019).

This paper aims to present the results of seismic analyses conducted on buckling restrained braced frames subjected to repeated earthquakes. 4-story and 10-story steel buckling restrained braced frames, representing the existing low to medium-rise BRBFs, were considered. The finite element 2D models of prototype BRBFs were created in Opensees (2014) and were subjected to five as-recorded seismic sequences. The seismic sequence ensemble was extracted from pacific earthquake engineering research center (PEER) ground motion database. Nonlinear time history analyses were conducted on prototype models and structural responses in terms of peak inter-story and residual drifts were acquired. Moreover, Park-Ang cumulative damage indices and global ductility demands were obtained.

2 Description of prototype buildings

Diagonally braced steel frames with pinned connections were considered for seismic analysis. A rectangular-shaped plan including four bays of 5 m in each direction and typical story height of 3.2 m were supposed for prototype buildings. The work-point to work-point length of braces was specified as 5940 mm, according to geometric specification of the braced frames. First, the prototypes were modeled and designed in Etabs (2016). 4-story

and 10-story diagonally braced residential buildings located on type III soil and in a very high seismicity zone with a PGA of 0.35 g, were considered. Composite steel deck floor system with dead and live loads of 3.5 and 3.8 KN/m, respectively, was assumed. Moreover, dead and live loads of 3 and 1.5 KN/m were specified for the roof. The external and the internal partition walls were supposed to impose dead loads of 1.5 KN/m and 1 KN/m, respectively. The grade 50 (ASTM A572) steel material with the yielding stress of 353 MPa and Poisson ratio of 0.3 was assumed for beams and columns. In addition, the yielding capacity and Young modulus of the core steel in BRBs were assumed as 370 MPa and 200 GPa, respectively. At the first step, the prototype buildings were designed per Iranian standard codes (2014). As a result, BRB core areas were determined considering prescribed loading combinations. Figure 1 illustrates the plan view and elevation of prototype buildings. In addition, Table 1 summarizes the seismic data of prototype building models. Moreover, Table 2 determines member sizes in buckling restrained braced frames. Tabulated values of R and C in Table 1 symbolize the response modification factor and base shear coefficient, respectively. Additionally, $T_{empirical}$ and $T_{analytical}$ correspondingly represent empirical and analytical period of BRBFs. According to Iranian seismic code (2014), the fundamental period of structure shall be taken as the minimum of $1.25T_{empirical}$ and $T_{analytical}$.

3 Modelling assumptions

Two-dimensional numerical models of 4-story and 10-story BRBFs were developed in *Opensees* software. As shown in Fig. 1a, the middle frame "C" was selected for the analysis. The geometric specifications of structural elements were specified per Table 2. *Nonlinear-beam-column* elements were identified for beams and columns. In addition, *corotational truss elements* were specified for BRBs. A pinned connection utilizing *zerolength* element was also specified at beams and columns ends. Dummy columns as

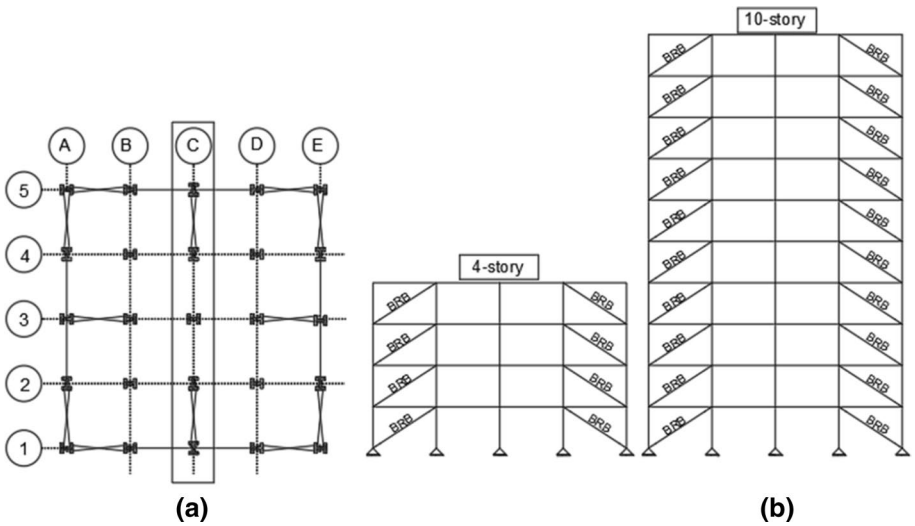

Fig.1 **a** Plan view, **b** Elevation view of buckling restrained braced frames

Table 1 Seismic parameters of prototype buildings

Seismic parameters	4-Story	10-Story
$PGA(g)$	0.35	0.35
R	7.0	7.0
C	0.14	0.12
$T_{empirical}\,(s)$	0.34	0.67
$1.25T_{empirical}\,(s)$	0.42	0.83
$T_{analytical}\,(s)$	0.82	1.50

Table 2 Member sizes of BRBFs

Model	Story	Column	Beam	BRB core area (cm^2)
4-Story	1	W12×53	W12×19	16
	2	W12×53	W12×19	14
	3	W12×35	W12×19	12
	4	W12×35	W12×19	7
10-Story	1	W12×230	W12×19	36
	2	W12×230	W12×19	36
	3	W12×230	W12×19	36
	4	W12×136	W12×19	34
	5	W12×136	W12×19	32
	6	W12×136	W12×19	28
	7	W12×136	W12×19	24
	8	W12×50	W12×19	20
	9	W12×50	W12×19	14
	10	W12×50	W12×19	8

elastic-beam-column elements, having moments of inertia and cross sectional areas considerably larger than frame columns, were employed to account for *P*-delta effects. *Zerolength* rotational spring elements with small stiffness were used to connect dummy columns to beam-column joints. Rigid links using *truss elements* were responsible for connection of dummy columns and the main frame, thus transferring the *P*-delta effects. The beam elements were supposed to sustain gravity loads tributary to the frame members while the remaining gravity loads were applied to the leaning columns. Inherent damping was modeled by *Rayleigh* damping via setting the critical damping ratio to 2% at the fundamental and third modes of the structure. Grade 50 steel with *steel02* material model was specified for all beams and columns. Furthermore, *SteelBRB* elastoplastic material model (Zona and Dall'Asta 2012) was identified for BRBs. Comparison between model prediction and experimental measurements conducted by Tremblay et al. (2006) is represented in Fig. 2.

Table 3 summarizes the *SteelBRB* material parameters. In Table 3, E and F_y denote the Young modulus and yielding stress of the core, respectively. Furthermore, $F^{+}_{y\max}$, $F^{-}_{y\max}$ characterize the maximum tension yield force of fully saturated isotropic hardening condition in tension and compression, respectively. $K^{+}_{0}, K^{-}_{0}, K^{+}_{1}$ and K^{-}_{1} correspondingly specify the initial stiffness in tension, initial stiffness in compression, post-yield stiffness in tension and post-yield stiffness in compression. Additionally, parameters δ^{+}_{r} and δ^{-}_{r} account for

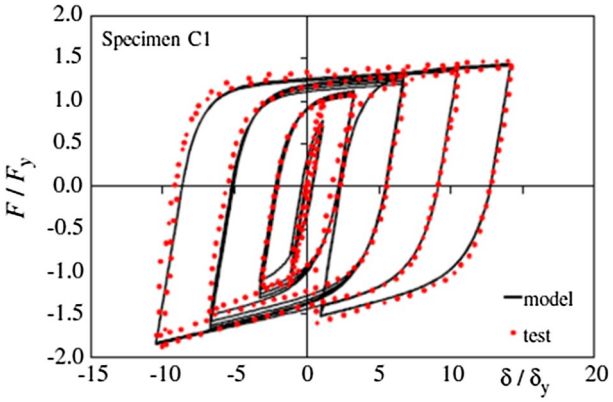

Fig. 2 Calibration of *SteelBRB* material model (Zona and Dall'Asta 2012)

Table 3 *SteelBRB* material parameters (Zona and Dall'Asta 2012)

E (GPa)	F_y (MPa)	$\frac{F^-_{y\max}}{F^+_{y\max}}$	$\frac{F^+_{y\max}}{F_y}$	δ^+_r	δ^-_r	α^+	α^-	$\frac{K^+_1}{K^+_0}$	$\frac{K^-_1}{K^-_0}$
200	370	1.18	1.33	0.2	0.1	0.9	0.9	0.01	0.04

hardening constants in tension and compression, respectively. The constants of plastic flow in tension and compression are specified by α^+ and α^-, respectively (Zona and Dall'Asta 2012).

The cross section of a BRB core is naturally variable over its length. An exact model of a BRB should reflect all parts of the core member serially connected together. However, for simplicity, the analytical model may be assumed as a single element, representative for core yielding portion, provided that an effective modulus of elasticity, E_{eff}, is proposed for the core steel material, as follows (Prinz and Richards 2012):

$$E_{eff} = E \cdot \frac{L_{tot}}{L_{yield}} \tag{1}$$

where L_{tot} and L_{yield} represent the work-point to work-point length of the BRB and the yielding length of the core, respectively. In this paper, a yielding length ratio of 0.7 was assumed for BRBs.

The rigid diaphragm at story levels was modeled using the constraint of equal degree of freedom of story nodes. A lumped mass system was considered in dynamic time history analysis. In addition, *P*-delta geometric transformation was assigned for beams and columns. Figure 3 represents the *Opensees* model of 4-story BRBF.

4 Mainshock-aftershock sequence

The strong ground motion database used in this paper consists of five real seismic sequences, which have been recorded in a short time period at the same site and station. The seismic sequences, extracted from PEER ground motion database, are summarized in Table 4. The records are compatible with soil type D, which was assumed for the design of prototype

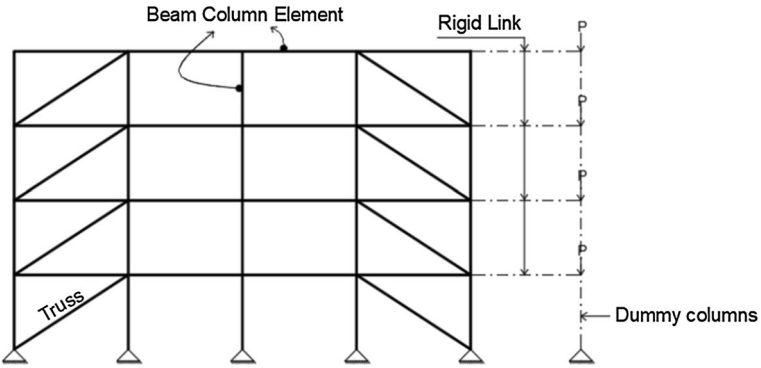

Fig. 3 The sketch of 2D BRBF model in *Opensees*

BRBFs. The seismic record ensemble includes *Mammoth lakes* (May 1980–2 events), *Chalfant valley* (July 1986, 2 events), *Coalinga* (July 1983, 2 events), *Northwest China* (April 1997, 2 events) and *Whittier Narrows* (October 1987, 2 events) earthquakes. Single ground motion records were combined to characterize sequential records. A time gap of 20 s with zero acceleration between single earthquake events was specified to assure the rest of structure at the end of mainshock and before the aftershock. Figure 4 illustrates the time histories of examined sequential records. The elastic spectra of the scaled ground motions for 4-story and 10-story BRBFs, considering 2% damping ratio, are also represented in Figs. 5 and 6, respectively. The phase 1 and phase 2 spectral accelerations in Figs. 5 and 6 correspond to mainshock and aftershock, respectively. For compatibility reasons with design procedure, seismic sequences were scaled to Design Basis Earthquake (DBE) target spectrum, according to Iranian seismic code of practice (2014). Similar scale factors were used for mainshock and consequent aftershocks, as shown in Table 4. As appears in Table 4, in all examined seismic sequences, the Peak Ground Acceleration (PGA) of the aftershock is greater than that of corresponding mainshock. By comparing the elastic spectra of seismic sequences in Fig. 4, it is evident that the spectral accelerations of *Coalinga*, *Chalfant valley* and *Northwest China* mainshock-aftershock sequences are similar to those of corresponding aftershocks, which demonstrates that the aftershock can control the response of structure. In contrast, in *Witter Narrows* and *Mammoth lakes* seismic events, the spectral accelerations of mainshock-aftershock sequences overlap the corresponding mainshocks. By knowing the fundamental period of 4-story BRBFs from modal analysis, which is determined as 0.8 s, it is evident that the spectral accelerations of seismic sequences of *Coalinga*, *Chalfant valley* and *Northwest China* events are greater compared with corresponding mainshocks, which implies that the earthquake recurrence tends to increase the seismic response of structure. However, as shown in Fig. 5, the spectral accelerations of *Whittier Narrows* and *Mammoth lakes* sequences, corresponding to fundamental period of 4-story BRBF, are smaller in comparison to corresponding mainshocks, which demonstrates that the mainshock controls the response and seismic demand on the structure would not be increased due to earthquake recurrence. Similar comparison can be made for 10-story BRBFs, by substituting the fundamental period of 1.5 s in spectral accelerations of earthquake scenarios illustrated in Fig. 6. It is worth mentioning that a non-degrading material behavior was assumed for BRBs in this research. Past studies have clarified that a BRB generally exhibits non-degrading response with positive post-yield stiffness under seismic events (Merrit et al. 2003; Tremblay et al. 2006; Ma et al. 2008). Typically, the governing

Table 4 Real seismic sequences

Nos.	Event	Station	Date	RSN[a]	Magnitude (M_w)	PGA (g)	NEHRP class	Scale factor	
								4-story BRBF	10-story BRBF
1	Mammoth lakes	Convict Creek	5/25/1980 (16:34)	230	6.1	0.44	D	3.10	4.80
			5/25/1980 (20:35)	240	5.7	0.48			
2	Chalfant valley	Brothers Ranch	7/20/1986 (14:29)	547	5.8	0.27	D	5.04	7.82
			7/21/1986 (14:42)	558	6.2	0.45			
3	Coalinga	46T04 CHP	7/22/1983 (02:39)	406	5.8	0.52	D	2.64	4.10
			7/25/1983 (22:31)	418	5.2	0.68			
4	Whittier narrows	24,401 San Marino	10/1/1987 (14:42)	691	6	0.19	D	7.08	10.98
			10/4/1987 (10:59)	716	5.3	0.21			
5	Northwest China	19,001 Jiashi, China	5/4/1997 (23:46)	1748	6.1	0.27	D	5.00	7.77
			11/4/1997 (5:34)	1752	5.9	0.30			

[a]Record sequential number

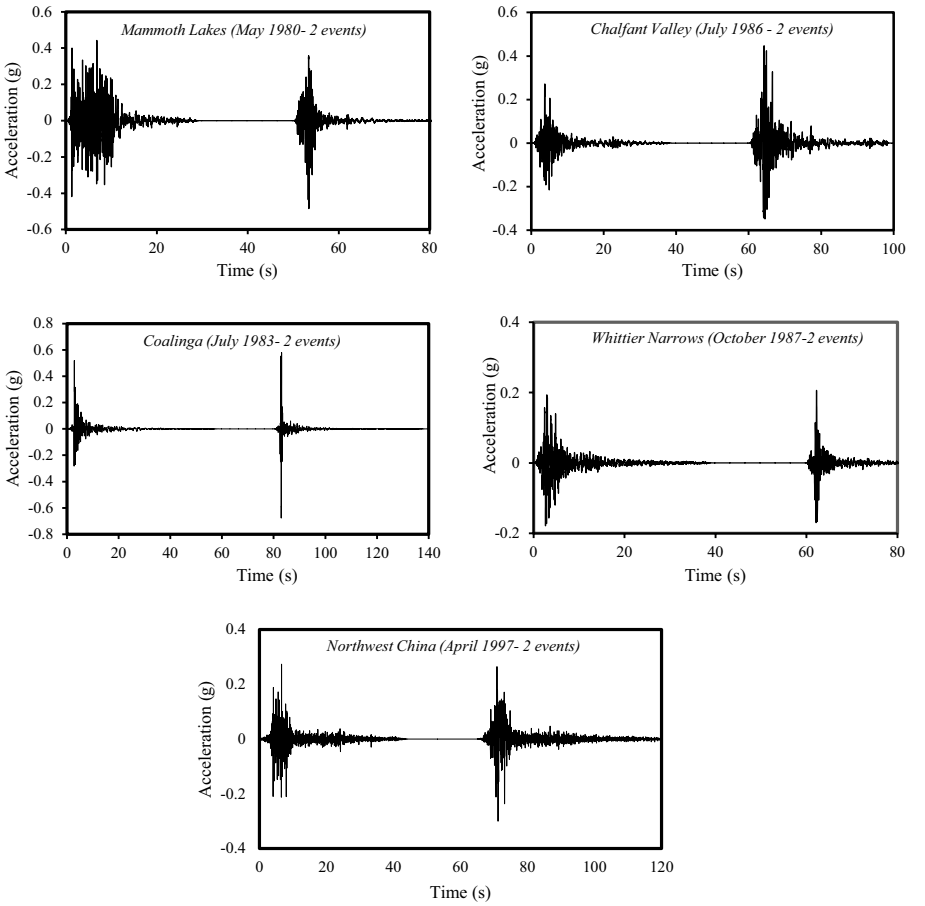

Fig. 4 Time histories of examined real seismic sequences

limit state in steel members that are expected to resist large seismic forces by sustaining large inelastic deformations is the ultra-low cycle fatigue (ULCF) fracture (Kanvinde and Deierlein 2007). In ULCF regime, fracture triggers due to a few (less than 20 cycles) large plastic strains. The void growth and coalescence-type mechanisms govern the physical processes of ULCF (Kanvinde and Deierlein 2007). Unfortunately, despite the ability to capture low cycle fatigue response, *Opensees* cannot predict ultra-low cycle fatigue fracture and thus other FEM programs like *ABAQUS* may be utilized to estimate ultra-low cycle fatigue life of BRBs via a micromechanics-based fatigue rules. Future studies may concentrate on seismic response of BRBs subjected to repeated earthquakes, considering ultra-low cycle fatigue response of the core member.

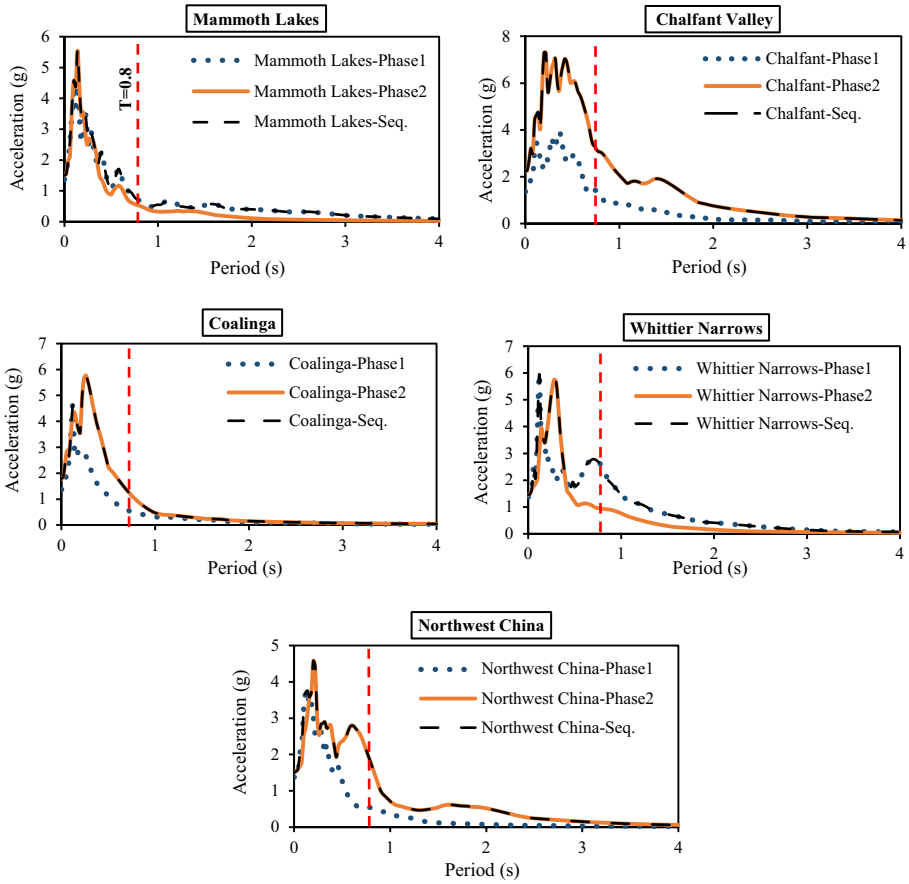

Fig. 5 Elastic response spectra of scaled seismic events for 4-story BRBF

5 Response of BRBFs under seismic sequence

In this section, inelastic responses of prototype 4-story and 10-story BRBFs subjected to examined mainshocks and mainshock-aftershock sequences are presented. For this purpose, first, the models were subjected to prescribed gravity loads and then the lateral loads were applied. Nonlinear time history analysis is a powerful tool to acquire dynamic structural responses under time-varying loading protocols, considering structural geometry and materials nonlinearity. To this end, the dynamic equilibrium equations are numerically solved by several methods like direct integration or modal techniques. The size of step time may noticeably affect the structural responses in direct-integration methods. Therefore, the step time should be reduced until results are not affected. Nonlinear time history analyses using Newmark's integration method were conducted in *Opensees* and structural responses in terms of Inter-Story Drift Ratio (ISDR) and Residual Drifts Ratio (RDR) were acquired. Figures 7 and 8 illustrate the height-wise distribution of ISDR and RDR demands in prototype models. As shown on Figs. 7 and 8, in both 4-story and 10-story BRBFs, the ISDR and RDR demands due to mainshock-aftershock sequences of *Chalfant valley*, *Coalinga* and *Northwest China*

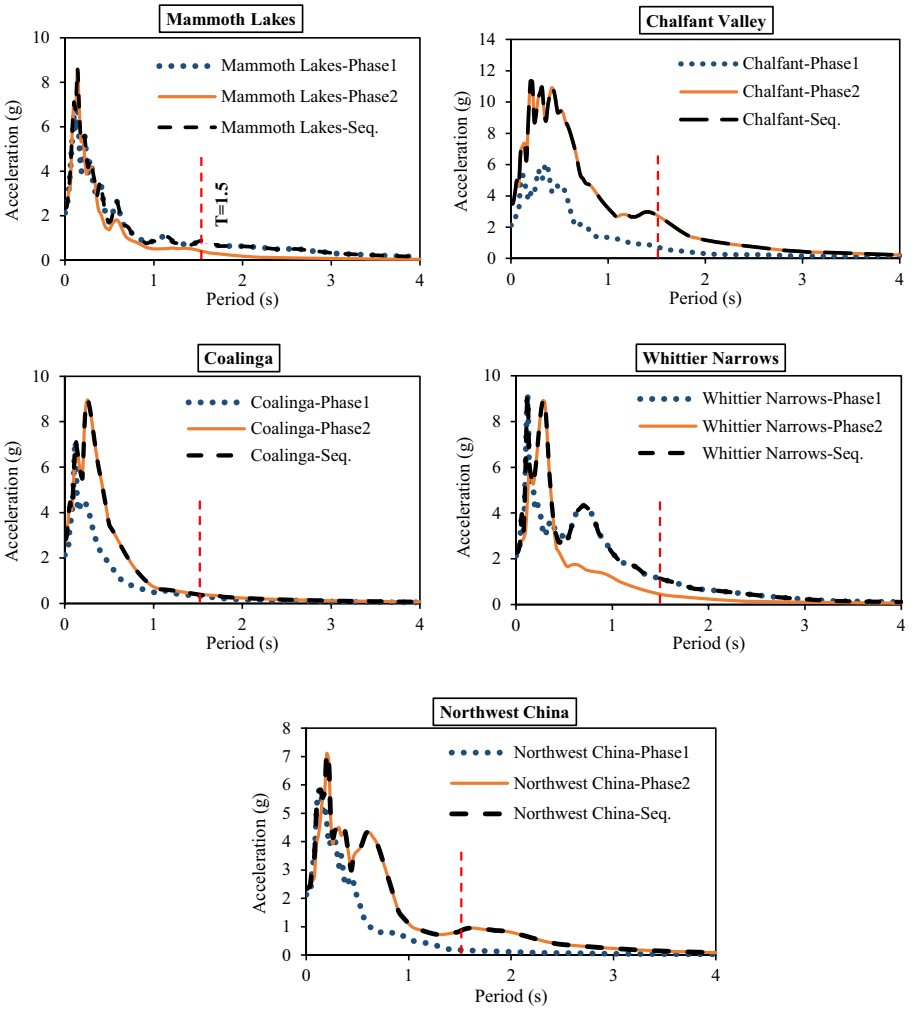

Fig. 6 Elastic response spectra of scaled seismic events for 10-story BRBF

earthquakes are relatively larger, in comparison to those of corresponding mainshocks. However, the mainshock-aftershock sequences of *Whittier Narrows* and *Mammoth lakes* do not significantly affect the response, since the spectral accelerations of their aftershocks remain below the spectral accelerations of corresponding mainshock-aftershock sequences, as shown in Figs. 5 and 6. The average ISDR and RDR demands are represented in Figs. 9 and 10. According to *FEMA356* (2000), the drift limit states for steel braced frame corresponding to collapse prevention (CP) and life safety (LS) limit states are 2% and 1.5%, respectively, while the corresponding residual drift ratios are 2% and 0.5%. The average ISDR demand of 4-story BRBF under examined mainshocks is 1.68%, which is below the CP limit state. The corresponding value for mainshock-aftershock sequence is around 2.6%, which indicates that the seismic sequences lead to larger drift response, in comparison with single events. The average ISDR under examined seismic sequences is around 1.46 times of the average ISDR under corresponding mainshocks, as shown in Fig. 9. Moreover, the comparison of average RDR

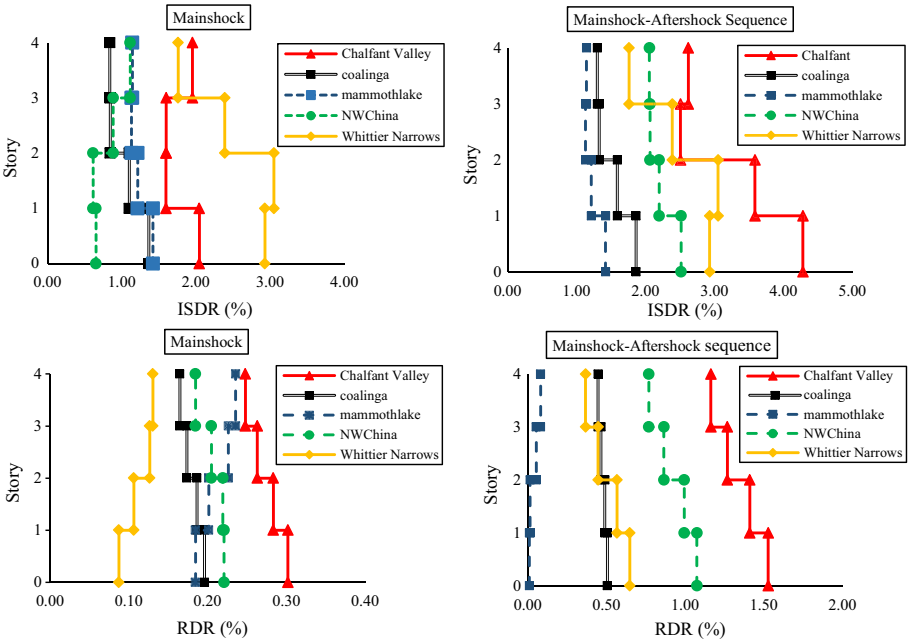

Fig. 7 Height-wise distribution of ISDR and RDR demands in 4-story BRBF

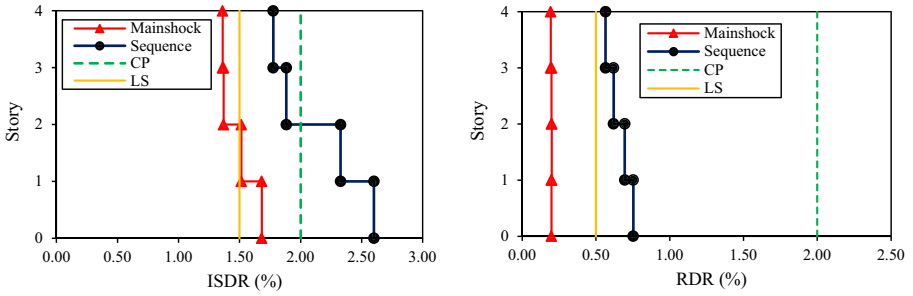

Fig. 8 Height-wise distribution of ISDR and RDR demands in 10-story BRBF

demands under mainshocks and mainshock-aftershock scenarios demonstrates that the seismic sequences considerably increase the permanent drift of structure. The average RDR demand of 4-story BRBF under examined mainshock-aftershock sequences is around 3.5 times of corresponding value under mainshock. Furthermore, the average RDR under seismic sequences exceeds the LS limit state, as shown in Fig. 9. Similar results are obtained for 10-story BRBFs subjected to as-recorded seismic events. As represented in Fig. 10, the average ISDR and RDR demands of 10-story BRBFs are significantly increased. The average ISDR of 10-story BRBF subjected to mainshock-aftershock sequences is 1.26 times of that of mainshocks. In addition, the ISDR demands under mainshock-aftershock sequence exceed the CP limit state. The peak average RDR demand of 10-story model under mainshock-aftershock sequence is around three times of that of mainshock. Additionally, the average RDR demand under seismic sequence exceeds the LS limit state, as appears in Fig. 10. In summary, the ISDR demands of

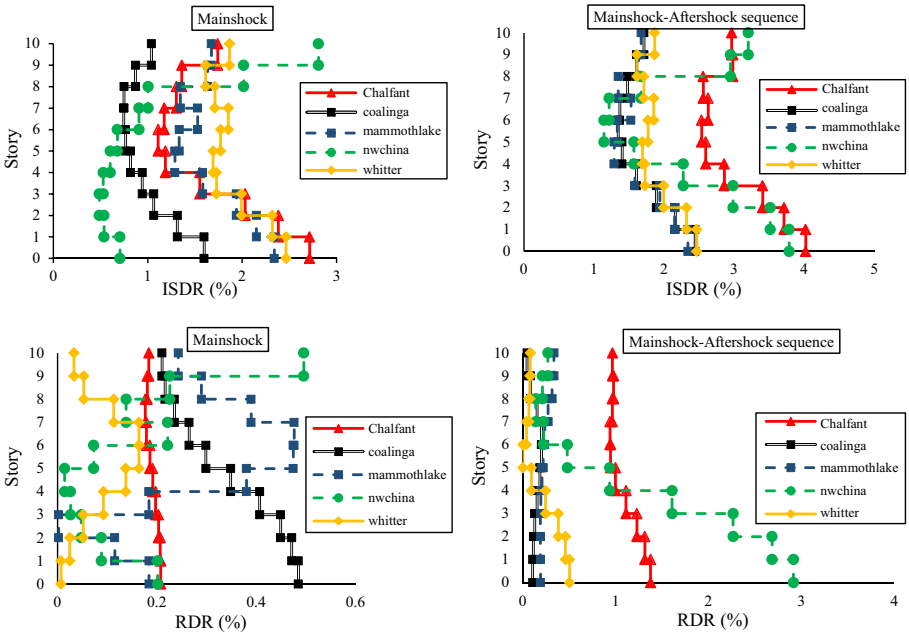

Fig. 9 Comparison of average ISDR and RDR demands in 4-story BRBF

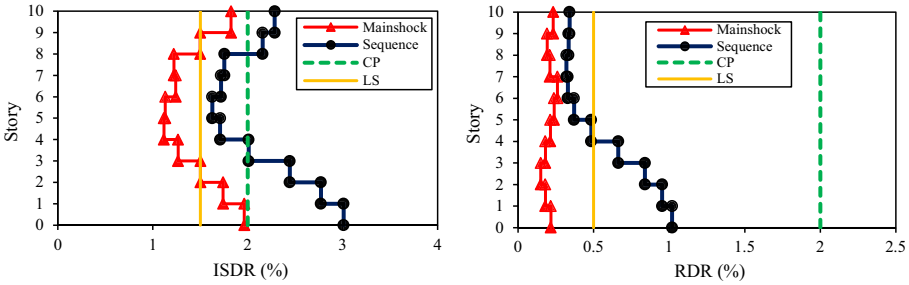

Fig. 10 Comparison of average ISDR and RDR demands in 10-story BRBF

4-story and 10-story prototype BRBFs under *Coalinga*, *Chalfant valley* and *Northwest China* sequences are significantly increased. However, since the spectral accelerations of *Mammoth lakes* and *Whittier Narrows* sequences, corresponding to fundamental period of examined BRBFs, are similar to those of corresponding mainshocks, they do not lead to increase of ISDR. Furthermore, it is found that the seismic sequence does not necessarily increase the RDR demands. In 4-story BRBF, the RDR demands are increased under all sequences, except the *Mammoth lake* earthquake. However, in 10-story BRBF, the RDR demands are kept constant under *Mammoth lakes* and *Coalinga* seismic sequences, compared with their corresponding mainshocks. The spectral acceleration of mainshock-aftershock sequence corresponding to fundamental period of structure, in comparison to that of mainshock, is found to be the most influential parameter that controls the peak drift response under seismic sequence. It is

evident that, due to the earthquake recurrence, increased average ISDR and RDR demands are required, in comparison with drifts for any of single event mainshocks.

6 Time histories of roof displacement

Time histories of roof displacements in 4-story and 10-story BRBFs under examined mainshocks, aftershocks and mainshock-aftershock sequences are correspondingly provided in Figs. 11 and 12. The peak roof displacement (PRD) under *Coalinga*, *Chalfant valley* and *Northwest China* mainshock-aftershock sequences are considerably greater compared with those of corresponding mainshocks, as represented in Table 5. However, the PRD demands are kept constant under seismic sequences of *Northwest China* and *Mammoth lakes*, since the response is controlled by the mainshock rather than the mainshock-aftershock sequence, as discussed earlier. The spectral accelerations of *Coalinga* mainshock and mainshock-aftershock sequence, corresponding to the fundamental period of 10-story BRBF, are very close together, as shown in Fig. 6, which can lead to similar peak roof displacements under mainshock and mainshock-aftershock sequence. However, the roof residual displacement at the end of *Coalinga* mainshock leads to larger displacement value under mainshock-aftershock sequence. In other words, the roof displacement of 10-story BRBF under *Coalinga* mainshock-aftershock is potentially increased due to the permanent displacement resulted from the mainshock, despite the spectral accelerations of mainshock and mainshock-aftershock sequence overlap at the fundamental period of examined structure. This phenomenon is only evident in *Coalinga* earthquake, while the spectral accelerations of other seismic sequences corresponding to the fundamental period of structure (i.e. 0.8 s for 4-story and 1.5 s for 10-story BRBF) are larger compared with those of corresponding mainshocks, as shown in Fig. 5. The residual roof displacement (RRD) demands of 4-story and 10-story BRBFs are summarized in Table 5. As appears in Table 5, in all examined BRBFs, except the 4-story BRBF under *Mammoth lake* earthquake and 10-story BRBF under *Coalinga* seismic sequences, the RRD demands under mainshock-aftershock sequences are significantly larger compared with those of corresponding mainshocks. Consequently, the earthquake recurrence does not necessarily increase the residual displacement of roof. It may depend on the frequency content of earthquake sequence. It is evident that, due to the recurrence of seismic events, amplified displacement demands are required. The maximum roof displacement for the case of *Northwest China* seismic sequence is increased by 300%, in comparison with the maximum displacement under single event earthquake, as shown in Table 5. The spectral acceleration of mainshock-aftershock sequence, compared with the spectral acceleration of single event mainshock, appears to control the peak roof displacement. From the results of this section, the amplified peak and permanent roof displacements under earthquake recurrence, which have not yet been addressed in existing building code of practice, should be taken into consideration for seismic design of buckling restrained braced frames.

7 Global ductility demand

The former section designated that while the spectral acceleration of mainshock–aftershock sequence, corresponding to fundamental period of structure, is greater compared with single event mainshock, the earthquake recurrence requires increased displacement

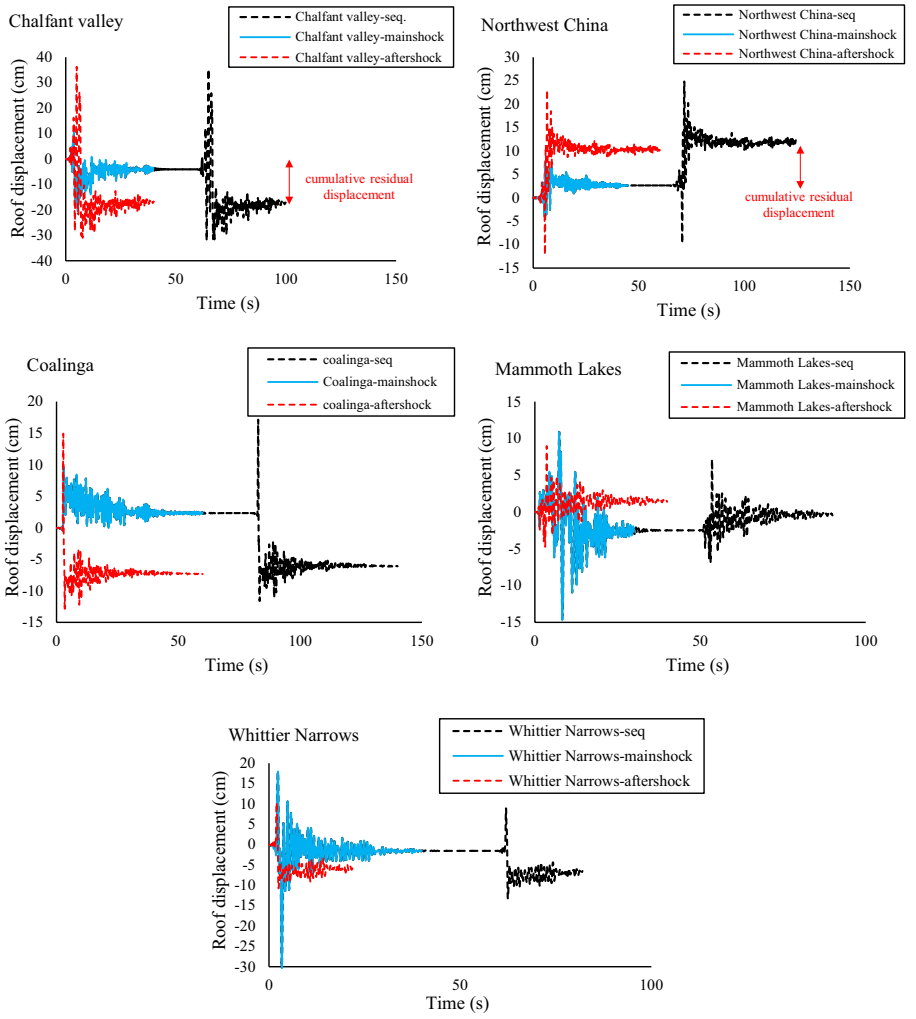

Fig. 11 Roof displacement time histories of prototype 4-story BRBFs

and ductility demands. The global ductility factor, μ, can be defined as the ratio of maximum roof displacement $u_{\max}$ and corresponding yielding displacement u_y (Chopra 2006), as follows:

$$\mu = \frac{u_{\max}}{u_y} \tag{2}$$

The global ductility demands of 4-story and 10-story BRBFs are evaluated and illustrated in Table 6. As appears in Table 6, the global ductility demands are significantly increased under mainshock-aftershock sequences of *Chalfant valley*, *Northwest China* and *Coalinga*. This implies that the BRBs are expected to experience larger ductility demands while subjected to repeated earthquakes. The increased ductility demands of BRBs under earthquake

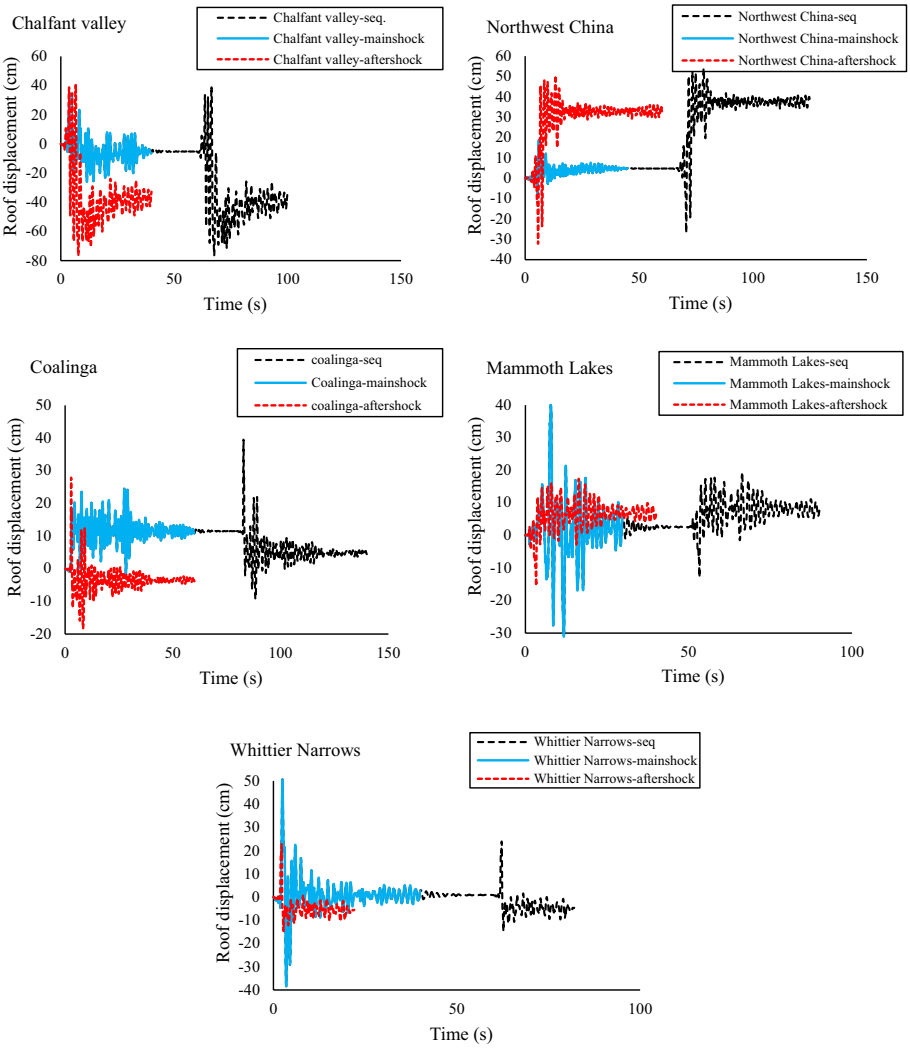

Fig. 12 Roof displacement time histories of 10-story BRBFs

recurrence affects the core strain demands, which may significantly reduce the ultra-low cycle fatigue fracture life of the core. As shown in Table 6, the global ductility demand remains approximately constant under *Mammoth lakes* and *Whittier Narrows* sequences, while it is increased by more than 300% under sequence of *Northwest China*. This outcome may be justified by the comparison of spectral accelerations of examined mainshocks and mainshock-aftershock sequences, similar to the discussions represented for inter-story and residual drift responses of BRBFs in previous sections of this paper.

Table 5 Peak and residual roof displacements under examined earthquakes

BRBF	Chalfant valley			Northwest China			Coalinga			Mammoth lakes			Whittier narrows		
	MS	AS	Seq	MS	AS	Seq	MS	AS	Seq	MS	AS	Seq	MS	AS	Seq
Peak roof displacement (cm)															
4-story	20.5	36.3	35.3	7.7	23.0	24.8	9.6	14.9	17.2	14.7	9.0	14.7	30.3	10.7	30.3
10-story	35.4	76.4	76.5	18.6	49.4	53.9	24.5	27.9	39.5	40.0	17.3	40.0	50.7	22.9	50.7
Residual roof displacement (cm)															
4-story	3.5	16.8	17.2	2.7	10.2	11.8	2.3	7.3	6.1	2.7	1.4	0.4	1.4	5.4	6.5
10-story	6.1	32.7	34.7	4.9	32.9	37.6	10.8	3.8	4.4	6.8	6.4	7.6	2.7	5.5	4.6

1-Mainshock, 2-Aftershock, 3-Mainshock-aftershock sequence

Table 6 Global ductility demands under examined earthquake scenarios

Events	Global ductility factor (μ)	
	4-story BRBF	10-story BRBF
Chalfant valley		
Mainshock	4.1	1.8
Sequence	7.1	3.8
Northwest China		
Mainshock	1.5	0.9
Sequence	5.0	2.7
Coalinga		
Mainshock	1.9	1.2
Sequence	3.4	2.0
Mammoth lakes		
Mainshock	2.9	2.0
Sequence	2.9	2.0
Whittier narrows		
Mainshock	6.1	2.5
Sequence	6.1	2.5

8 Determination of cumulative damage

The well-known Park-Ang damage index (DI) for structural elements is calculated per seismic event. The damage index proposed by Park and Ang (1985) is a combination of hysteretic energy and maximum displacement demand, as in the following:

$$DI = \frac{\delta_m}{\delta_u} + \frac{\beta}{\delta_u P_y} \int dE_h \tag{3}$$

where δ_m and δ_u correspondingly designate the maximum and the ultimate deformation of the element. Furthermore, β is a constant to control strength deterioration, which is assumed as 0.15 in this study (Kaveh et al. 2014). The term $\int dE_h$ denotes hysteretic energy dissipated by the element during the seismic event and P_y represents the yield strength of the element. In this study, it is assumed that the damage is localized only in BRB elements. The global damage index, which is a combination of local damage indices, can be estimated as follows (Vasilopoulos and Beskos 2006):

$$DI_G = \frac{\sum_1^m DI_i^2}{\sum_1^m DI_i} \tag{4}$$

in which DI_G represents the global damage index and DI_i signifies the local damage index of member "i". The global damages in terms of Park-Ang damage index under examined seismic events are summarized in Table 7. As shown in Table 7, the damage indices of 4-story and 10-story BRBFs under *Northwest China*, *Chalfant valley* and particularly *Coalinga* sequences are increased, compared with single event mainshocks. However, the damage indices remains constant for BRBFs subjected to *Mammoth Lakes* and *Whittier Narrows* sequences. The Park-Ang damage index for different levels of performance is represented in Table 8. Considering the data provided in Table 8, the damage indices under

Table 7 Park-Ang global damage indices

Nos.	Event	Global damage index	
		4-story	10-story
1	Chalfant valley (MS[1])	0.10	0.10
2	Chalfant valley (Seq[2])	0.28	0.25
3	Northwest China (MS)	0.04	0.11
4	Northwest China (Seq)	0.11	0.17
5	Coalinga (MS)	0.04	0.04
6	Coalinga (Seq)	0.07	0.07
7	Mammoth lakes (MS)	0.07	0.09
8	Mammoth lakes (Seq)	0.08	0.10
9	Whittier narrows (MS)	0.13	0.10
10	Whittier narrows (Seq)	0.14	0.11

1-Mainshock; 2-Sequence

Table 8 Park-Ang damage index for different performance levels

Park-Ang damage index	Performance level
0–0.2	IO
0.2–0.5	LS
0.5–0.8	CP

Chalfant valley sequence exceeds the immediate occupancy (IO) limit state, while the damage states remain below the IO limit state in other cases. The increased damage index of prototypes under *Northwest China*, *Chalfant valley* and especially *Coalinga* sequences can be related to higher energy dissipation capacity and ductility of structure under mentioned seismic sequence. As a result, the earthquake recurrence has the potential to significantly increase the cumulative damage index and change the performance level of structures. Nevertheless, the global damage index is only surveyed for idealized single event earthquakes in most of existing seismic codes.

9 Summary and conclusion

Repeated earthquakes can significantly affect the structural response. Unlike steel moment-resisting frames, performance of buckling restrained braced frames under real seismic sequences has not been addressed sufficiently in the literature. This paper examines the seismic response of steel buckling restrained braced frames under earthquake recurrence. For this purpose, five real seismic events downloaded from PEER ground motion database were considered. 4-story and 10-story buckling restrained braced frames were subjected to mainshock and mainshock-aftershock earthquake scenarios. Nonlinear time history analyses were conducted and structural responses in terms of peak and residual drifts were acquired. Furthermore, global ductility demands and cumulative damage indices were

calculated per seismic event. According to the analyses results, following conclusions can be drawn:

1. The seismic sequence does not necessarily require increased peak inter-story drift, cumulative damage index and global ductility demands in BRBFs. It appears to be associated with spectral acceleration of seismic events. In the case of larger spectral acceleration of mainshock-aftershock sequence corresponding to the fundamental period of examined structure, compared with that of single event mainshock, the seismic sequence can considerably increase the peak inter-story, global ductility demand and cumulative damage index of buckling restrained braced frame.
2. The residual displacement demands under seismic sequence are not certainly increased, compared with single event mainshock. In other words, the seismic sequence may increase or decrease the permanent displacements, which can be attributed to the frequency content of the seismic record.
3. The average peak inter-story drifts of 4-story and 10-story BRBFs under examined seismic sequences are increased by 46 and 25%, respectively. The average residual drifts appears to be increased by more than 300% under sequential ground motions.
4. The cumulative damage index and the performance level of BRBFs can be potentially altered due to earthquake recurrence. The park-Ang damage index can be significantly increased due to amplified cumulative hysteretic energy and displacement demands under earthquake recurrence.
5. The large permanent drift of structure at the end of mainshock can significantly increase the peak inter-story drift demand under aftershock. The spectral acceleration of seismic sequence compared with single event mainshock and permeant drift at the end of mainshock are specified as two essential parameters that control the response under sequential ground motions.

References

Abdollahzadeh G, Sadeghi A (2018) Earthquake recurrence effect on the response reduction factor of steel moment frame. Asian J Civ Eng. https://doi.org/10.1007/s42107-018-0079-3

Aki K (1984) Asperities, barriers, characteristic earthquakes and strong motion prediction. J Geophys Res 89:5867–5872

Amadio C, Fragiacomo M, Rajgelj S (2003) The effects of repeated earthquake ground motions on the nonlinear response of SDOF systems. Earthq Eng Struct Dynam 32:291–308

Avci-Karatas C, Celik O, Yalcin C (2018) Experimental investigation of aluminum alloy and steel core buckling restrained braces (BRBs). Int J Steel Struct Springer 18(2):650–673. https://doi.org/10.1007/s13296-018-0025-y

Avci-Karatas C, Celik OC, Eruslu SO (2019) Modeling of buckling restrained braces (BRBs) using full-scale experimental data. KSCE J Civ Eng Springer 23(10):4431–4444. https://doi.org/10.1007/s12205-019-2430-y

Black CJ, Makris N and Aiken ID (2000) Component testing, stability analysis and characterization of buckling restrained braced frames. PEER Report No 8, Berkeley, CA.

Celik OC, Yuksel E, Avci-Karatas C, Bal A, Gokce T, Bago Z, Koller G (2015) Component testing of steel-core buckling restrained braces (BRBs) with pinned end connections. The 8th International conference on advances in steel structures (ICASS-2015), July 21–24, Lisbon, Portugal.

Chopra A (2006) Dynamics of structures: theory and applications to earthquake engineering, 3rd edn. Prentice Hall Inc, New Jersey

Dalguer L. A., Miyake H and Irikura K (2002) Characterization of dynamic asperity source models for simulating strong ground motion. Proc. 13th World conference on earthquake engineering, Paper No. 3286, Vancouver, Canada

Diaz-Martinez G, Ruiz-Garcia J, Teran-Gilmore A (2014) Response of structures to seismic sequences corresponding to Mexican soft soils. Earthq Struct 7:1241–1258

Etabs (2016) Integrated software package for the structural analysis and design of buildings, Computers and structures, Inc. (CSI).California

Fahnestock L, Ricles J, Sause R (2007) Experimental evaluation of a large-scale buckling-restrained braced frame. J Struct Eng 133:1205–1214

FEMA-356 (2000) Pre-standard and commentary for the seismic rehabilitation of buildings, ASCE, Federal emergency management agency, Washington D.C.

Fragiacomo M, Amadio C, Macorini L (2004) Seismic response of steel frames under repeated earthquake ground motions. Eng Struct 26:2021–2035

Guerrero H, Ruíz-García J, Alberto Escobar J, Terán-Gilmore A (2017) Response to seismic sequences of short-period structures equipped with buckling-restrained braces located on the lakebed zone of Mexico City. J Constr Steel Res 137:37–51

Guo Y, Tong J, Zhang B, Zhu B, Pi Y (2017) Theoretical and experimental investigation of core-separated buckling-restrained braces. J Constr Steel Res. 135:137–149

Hatzigeorgiou GD, Beskos DE (2009) Inelastic displacement ratios for SDOF structures subjected to repeated earthquakes. Eng Struct 31:2744–2755

Hatzigeorgiou GD (2010) Ductility demand spectra for multiple near- and far-fault earthquakes. Soil Dyn Earthq Eng 30:170–183

Hatzigeorgiou GD, Liolios AA (2010) Nonlinear behavior of RC frames under repeated strong ground motions. Soil Dyn Earthq Eng 30:1010–1025

Hoveidae N, Rafezy B (2012) Overall buckling behavior of all-steel buckling restrained braces. J Constr Steel Res. 79:51–158

Hoveidae N, Habibi Pourzare B (2019) Comparison of progressive collapse capacity of steel moment resisting frames and dual systems with buckling restrained braces. J Rehabil Civ Eng 7(4):37–56

Iranian code of practice for seismic resistant design of buildings (2014) Standard No. 2800, 4th Edition Building and housing research center, Tehran, Iran.

Kanvinde A, Deierlein G (2007) Cyclic void growth model to assess ductile fracture initiation in structural steels due to ultra-low cycle fatigue. J Struct Eng 133(6):701–712

Kaveh A, Kalateh-Ahani M, Fahimi-Farzam M (2014) Damage-based optimization of large-scale steel structures. Earthq Struct 6:1119–1139

Lee K, Foutch DA (2004) Performance evaluation of damaged steel frame buildings subjected to seismic loads. J Struct Eng 130:588–599

Li Q, Ellingwood BR (2007) Performance evaluation and damage assessment of steel frame buildings under main shock-aftershock sequences. Earthq Eng Struct Dyn 36:405–427

Liolios A, Hatzigeorgiou G (2013) A numerical approach for estimating the effects of under multiple earthquakes to seismic response of structures strengthened by cable-elements. J Theor Appl Mech 43(3):21–32

Liolios A, Elenas A, Liolios A, Radev S, Georgiev K, Georgiev I (2015) Tall RC Buildings environmentally degradated and strengthened by cables under multiple earthquakes: A numerical approach. In: Dimov I, Fidanova S, Lirkov I (eds) Numerical methods and applications. NMA 2014. Lecture notes in computer science, vol 8962. Springer, Cham

Loulelis D, Hatzigeorgiou GD, Beskos DE (2012) Moment resisting steel frames under repeated earthquakes. Earthq Struct 3:231–248

Luco N, Bazzurro P and Cornell CA (2004) Dynamic versus static computation of the residual capacity of mainshock-damaged building to withstand an aftershock. Proc 13th World conference on earthquake engineering, Paper No. 2405, Vancouver, Canada

Mahin SA (1980) Effects of duration and aftershocks on inelastic design earthquakes. Proc of the seventh world conference on earthquake engineering, Istanbul 5: 677–679

Ma N, Wu B, Zhao J, Li H, Yang W (2008) Full-scale test of all-steel buckling restrained braces. 14th world conference on earthquake engineering, Beijing, China

Massumi A, Absalan M (2013) Interaction between bracing system and moment resisting frame in braced RC frames. Archives Civ Mech Eng 13:260–268

Merrit S, Uang C, Benzoni G (2003) Subassemblage testing of corebrace buckling-restrained braces, Final Report to Core Brace, LLC. Report No. TR-2003/0

Morfuni F, Freddi F, Galasso C (2019) Seismic performance of dual systems with BRBs under mainshock-aftershock sequences. 13th International conference on applications of statistics and probability in civil engineering, ICASP13 Seoul, South Korea

OpenSEES (2014) Open system for earthquake engineering simulation. Pacific earthquake engineering research center, University of California, Berkeley, California

Park YJ, Ang AHS (1985) Mechanistic seismic damage model for reinforced concrete. J Struct Eng ASCE 111(4):722–739

Prinz GS, Richards PW (2012) Seismic performance of buckling-restrained braced frames with eccentric configurations. J Struct Eng 138(3):345–353

Ruff F, Kanamori H (2003) The rupture process and asperity distribution of three great earthquakes from long-period diffracted P-waves. Phys Earth Planet Inter 31:202–230

Ruiz-García J, Negrete-Manriquez JC (2011) Evaluation of drift demands in existing steel frames under as-recorded far-field and near-fault mainshock–aftershock seismic sequences. Eng Struct 33:621–634

Ruiz-García J (2012) Mainshock-aftershock ground motion features and their influence in building's seismic response. J Earthq Eng 16:719–737

Ruiz-García J, Yaghmaei-Sabegh S, Bojórquez E (2018) Three-dimensional response of steel moment-resisting buildings under seismic sequences. Eng Struct 175:399–414

Sabelli R, Mahin S, Chang C (2003) Seismic demands on steel braced frame buildings with buckling restrained braces. Eng Struct 5:655–666

Tremblay R, Bolduc P, Neville R, Devall R (2006) Seismic testing and performance of buckling-restrained bracing systems. Can J Civ Eng 33:183–198

Vasilopoulos AA, Beskos DE (2006) Seismic design of plane steel frames using advanced methods of analysis. Soil Dyn Earthq Eng 26(12):1077–1100

Zona A, Dall'Asta A (2012) Elastoplastic model for steel buckling-restrained braces. J Constr Steel Res 68:118–125